Eur. Phys. J. C 21, 473–488 (2001)
Digital Object Identifier (DOI) 10.1007/s100520100754

THE EUROPEAN PHYSICAL JOURNAL C

The pion–nucleon scattering lengths from pionic hydrogen and deuterium

H.-Ch. Schröder[1], A. Badertscher[1,a], P.F.A. Goudsmit[1], M. Janousch[1], H.J. Leisi[1,b], E. Matsinos[1], D. Sigg[1], Z.G. Zhao[1], D. Chatellard[2], J.-P. Egger[2], K. Gabathuler[3], P. Hauser[3], L.M. Simons[3], A.J. Rusi El Hassani[4]

[1] ETH Zurich, Institute for Particle Physics, 8093 Zurich, Switzerland
[2] Institut de Physique de l'Université de Neuchâtel, 2000 Neuchâtel, Switzerland
[3] Paul Scherrer Institut, 5232 Villigen PSI, Switzerland
[4] Department de Physique, Faculté des Sciences et Téchnique, Tanger, Morocco

Received: 20 April 2001 / Revised version: 6 July 2001 /
Published online: 24 August 2001 –

Abstract. This is the final publication of the ETH Zurich–Neuchâtel–PSI collaboration on the pionic hydrogen and deuterium precision X-ray experiments. We describe the recent hydrogen $3p$–$1s$ measurement, report on the determination of the Doppler effect correction to the transition line width, analyze the deuterium shift measurement and discuss implications of the combined hydrogen and deuterium results. From the pionic hydrogen $3p$–$1s$ transition experiments we obtain the strong-interaction energy level shift $\varepsilon_{1s} = -7.108 \pm 0.013(\text{stat.}) \pm 0.034(\text{syst.})\,\text{eV}$ and the total decay width $\Gamma_{1s} = 0.868 \pm 0.040(\text{stat.}) \pm 0.038(\text{syst.})\,\text{eV}$ of the $1s$ state. Taking into account the electromagnetic corrections we find the hadronic πN s-wave scattering amplitude $a_{\pi^- p\to\pi^- p} = 0.0883 \pm 0.0008 m_\pi^{-1}$ for elastic scattering and $a_{\pi^- p\to\pi^0 n} = -0.128 \pm 0.006 m_\pi^{-1}$ for single charge exchange, respectively. We then combine the pionic hydrogen results with the $1s$ level shift measurement on pionic deuterium and test isospin symmetry of the strong interaction: our data are still compatible with isospin symmetry. The isoscalar and isovector πN scattering lengths (within the framework of isospin symmetry) are found to be $b_0 = -0.0001^{+0.0009}_{-0.0021} m_\pi^{-1}$ and $b_1 = -0.0885^{+0.0010}_{-0.0021} m_\pi^{-1}$, respectively. Using the GMO sum rule, we obtain from b_1 a new value of the πN coupling constant ($g_{\pi N} = 13.21^{+0.11}_{-0.05}$) from which follows the Goldberger–Treiman discrepancy $\Delta_{\text{GT}} = 0.027^{+0.012}_{-0.008}$. The new values of b_0 and $g_{\pi N}$ imply an increase of the nucleon sigma term by at least 9 MeV.

1 Introduction

Quantum chromodynamics (QCD) is considered to be the fundamental theory of the strong interactions. Important symmetry properties of the theory, namely the chiral and the isospin symmetry, can only be tested at *low energies*.

QCD reveals the spontaneous breakdown of chiral symmetry (also referred to as a "hidden symmetry"): the ground state is less symmetric than the hamiltonian of the theory. In QCD with massless u- and d-quarks, the hamiltonian is symmetric with respect to the chiral-symmetry group $SU(2)_{\text{R}} \times SU(2)_{\text{L}}$ which breaks down to the isospin-symmetry group $SU(2)$ in the ground state [1]. In this approximation, there are three massless Goldstone bosons (π^-, π^0, π^+). In a next step, the (small) u- and d-quark masses are turned on; as a result the pion acquires mass (M_π). *Chiral perturbation theory* (ChPT), which is an expansion in terms of M_π and momenta, can then be used to calculate the low-energy hadronic properties in terms of low-energy constants (LEC's). ChPT provides the link between the experimental data and QCD. Since the u- and d-quark masses are different, there is – at some level – breaking of the isospin symmetry of the strong interaction.

Recently, substantial progress has been made in developing ChPT for the pion–nucleon (πN) system [2–8]. In this context the precision X-ray experiments on pionic hydrogen [9,10] and pionic deuterium [11], carried out by the ETH Zurich–Neuchâtel–PSI collaboration, are of particular relevance for the following reasons. The results from these experiments lead to a test of isospin symmetry directly at threshold (without the need to extrapolate in energy) where the ChPT is supposed to work best. Within the framework of isospin symmetry, we obtain directly measured and precise πN (s-wave) scattering lengths; these can be confronted with recent ChPT work. The isovector scattering length allows a new determination of the πN coupling constant from which the Goldberger–Treiman discrepancy is determined, testing

[a] *Corresponding author:* Badertscher@particle.phys.ethz.ch
[b] e-mail: Leisi@particle.phys.ethz.ch

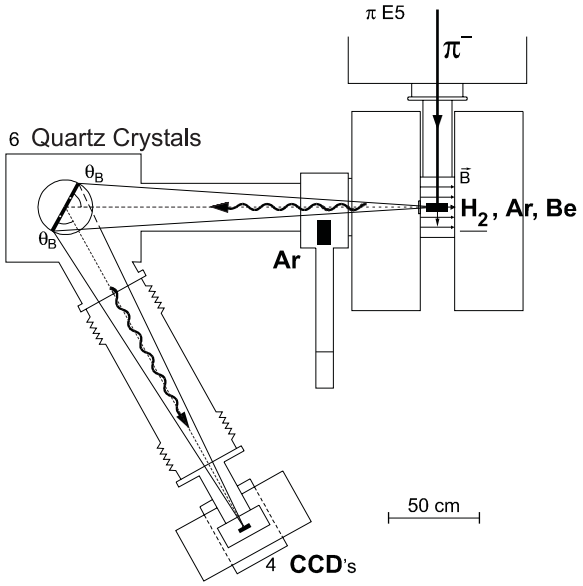

Fig. 1. Experimental setup. Pion beam ($\pi E5$), cyclotron trap with target cell (H_2, Ar, Be), argon X-ray source for stability monitoring (Ar), bent crystals of spectrometer (quartz(110)) with Bragg angle (Θ_B) and detector system (CCD's)

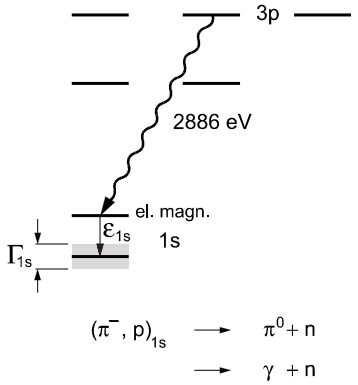

Fig. 2. Schematic level diagram of pionic hydrogen with the $3p$–$1s$ X-ray transition and the decay of the $(\pi^-, p)_{1s}$ ground state. The strong-interaction shift ε_{1s} for pionic hydrogen is negative (attractive interaction)

the chiral expansion. The nucleon sigma term (a quantity accessible to ChPT and lattice calculations) is sensitively affected by the new isoscalar scattering length.

In the present paper, we describe important details on which the final results of our collaboration are based, and draw conclusions from these results. In Sect. 2, the most recent measurement of the $3p$–$1s$ X-ray transition in pionic hydrogen [12] is reported in detail. A new way of determining the Doppler effect which is needed for relating the measured line width to the decay width of the 1s ground state is presented in Sect. 3, and compared with earlier evaluations. We then combine (in Sect. 4) all pionic hydrogen results with the strong-interaction shift measurement of pionic deuterium [11], test isospin symmetry and evaluate the πN scattering lengths. The implications of the results will be discussed in detail.

2 Experiment and data analysis

2.1 Conception of the experiment

The measurement of the pionic hydrogen $3p$–$1s$ X-ray transition was performed at the low-energy pion beam ($\pi E5$) of the Paul Scherrer Institute (PSI) [12] with the crystal spectrometer system described in [9,11,13] (see Fig. 1). Pions from the $\pi E5$ beam at PSI are degraded inside the cyclotron trap [14] which is a magnetic field device designed to increase the stop density in the target cell at its center. The X-rays from the target cell are measured with two bent crystal spectrometers mounted on top of each other (with three quartz (110) crystals each). The X-ray detector system consists of an array of charge coupled devices (CCD's) with a total of 3.6 million pixels. In addition to the cryogenic gaseous H_2 target cell (15 bar equivalent), an argon electronic X-ray source for energy calibration and one for stability monitoring (Ar in Fig. 1), together with a beryllium pionic X-ray target for measuring the spectrometer resolution curve (Be in Fig. 1) are used.

The transition energy ($E^{\text{meas.}}_{3p\text{-}1s}$) was determined by measuring the Bragg angle difference relative to the well-known electronic argon $K_{\alpha 1}$ X-ray line [15]. The *strong-interaction shift* ε_{1s} is defined by (see Fig. 2)

$$\varepsilon_{1s} = E^{\text{el.mag.}}_{3p\text{-}1s} - E^{\text{meas.}}_{3p\text{-}1s}, \tag{1}$$

where $E^{\text{el.mag.}}_{3p\text{-}1s}$ is the electromagnetic transition energy calculated in the absence of the strong interaction [16] (the strong-interaction shift of the $3p$ state is negligible). The shift ε_{1s}, thus defined, is not yet a purely hadronic quantity. In order to arrive from ε_{1s} at the hadronic s-wave amplitude $a_{\pi^- p \to \pi^- p}$ for elastic $\pi^- p$ scattering, the so-called *electromagnetic corrections* have to be applied [16]. These include the change of the transition energy due to the modification of the pion wave function by the strong-interaction potential, the mass-splitting effect (the continuum final states (π^0, n) of the decaying (π^-, p) $1s$ bound state modify slightly the energy of the bound state) and the corresponding effect with the continuum final states (γ, n) (Fig. 2). In [16] the relation between ε_{1s} and $a_{\pi^- p \to \pi^- p}$ was established numerically, by using an attractive strong-interaction potential for the isospin 1/2 channel and a repulsive potential for isospin 3/2. Isospin symmetry of the strong interaction is assumed throughout the analysis. The strong-interaction pion mass (M_π) is assigned (by convention) to be that of the (physical) charged pion $m_\pi = 139.56995 \pm 0.00035\,\text{MeV}$. The result can be expressed for convenience in terms of an electromagnetic correction $\delta_\varepsilon = (-2.1 \pm 0.5) \times 10^{-2}$ to a Deser-type formula [17]:

$$\frac{\varepsilon_{1s}}{E_{1s}} = -4 \frac{a_{\pi^- p \to \pi^- p}}{r_B} (1 + \delta_\varepsilon), \tag{2}$$

where E_{1s} is the point-Coulomb electromagnetic binding energy of the $1s$ level and $r_B = 222.6\,\mathrm{fm}$ the Bohr radius; $E_{1s}/r_B = 14.53\,\mathrm{eV/fm}$[1].

The transition line width ($\Gamma^{\mathrm{meas.}}_{3p\text{-}1s}$) was determined by deconvoluting the measured line shape with the instrumental resolution function of the spectrometer (Sect. 2.4). The resolution function is obtained from a measurement of the $4f$–$3d$ X-ray line of pionic beryllium of which the natural line width is very small. The quantity $\Gamma^{\mathrm{meas.}}_{3p\text{-}1s}$ is dominated by the decay width Γ_{1s} of the $1s$ state. It is, however, affected by the Doppler broadening of the $3p$ initial state of the X-ray transition (see Sect. 3). Since the natural width of the $3p$ state is negligibly small, the relation between the measured line width and the decay width of the $1s$ state depends on the Doppler effect only. We define this relation by the equation

$$\frac{\Gamma^{\mathrm{meas.}}_{3p\text{-}1s}}{\Gamma_{1s}} = 1 + \Delta_{3p}. \tag{3}$$

Section 3 is devoted to an evaluation of the Doppler correction Δ_{3p}.

The total decay width Γ_{1s} of the $1s$ state is determined by the rate of the single charge exchange (SCX) reaction $(\pi^- p)_{1s} \to \pi^0 n$ and the radiative decay $(\pi^- p)_{1s} \to \gamma n$ (Fig. 2). The ratio of the two decay rates is the Panofsky ratio $P = 1.546 \pm 0.009$ [19]. Using this value we can thus express Γ_{1s} in terms of the hadronic s-wave amplitude $a_{\pi^- p \to \pi^0 n}$ for SCX scattering. In addition, we take into account the (small) electromagnetic corrections [16]. As explained above, the relation between Γ_{1s} and $a_{\pi^- p \to \pi^0 n}$ was investigated in [16] numerically. The result can again be expressed in terms of an electromagnetic correction $\delta_\Gamma = (-1.3 \pm 0.5) \times 10^{-2}$ to a Deser-type formula:

$$\frac{\Gamma_{1s}}{E_{1s}} = 8\frac{q}{r_B}\left(1 + \frac{1}{P}\right)\left[a_{\pi^- p \to \pi^0 n}(1 + \delta_\Gamma)\right]^2, \tag{4}$$

where $q = 28.04\,\mathrm{MeV}/c$ (equivalent to $0.1421\,\mathrm{fm}^{-1}$ in units $\hbar = c = 1$) is the center of mass momentum of the π^0 in the SCX reaction.

2.2 Experimental improvements

The improvements in the present experiment [12] as compared to the earlier measurements [9] are listed here.

An increase of the pionic X-ray rate (by a factor of two) resulted from an optimized tune of the beam line and the cyclotron trap, together with the enhanced primary proton current. Three times more events were collected. The signal-to-noise was improved by a factor of two, as a result of the shielding of the CCD's with aluminium foils against the steel flange of their mounting (in order to reduce the iron and chromium X-ray lines) and a massive shielding between spectrometer and $\pi E5$ beam line.

A new beryllium target was built, consisting of ten 0.02 mm thick, 40 mm diameter beryllium foils mounted in parallel. The surfaces of the foils were nearly perpendicular to the direction target-cell–bent crystal (see Fig. 1) but slightly tilted, in order to maximize the average amount of beryllium seen by the incident pions.

An improvement of the spectrometer resolution was achieved by a careful alignment of the individual crystals, using the electronic $K_{\alpha 1}$ X-ray line of zinc (8.6 keV) in 3rd order Bragg reflection. This line matches the $3p$–$1s$ pionic hydrogen line nearly exactly in angle.

The long term geometrical and thermal stabilities have been carefully investigated and controlled during the entire measuring period, e.g. with frequent argon calibration measurements. From a temperature measurement in the vicinity of the crystals we conclude that the effect of lattice spacing variation with temperature corresponded to a variation in energy of less than 1 meV.

The lattice constants of all individual crystals of the spectrometer have been measured in the bent state; all measured values were within the uncertainties given in (11).

2.3 Event selection and position spectra

CCD's with a pixel size of $22.5\,\mu\mathrm{m} \times 22.5\,\mu\mathrm{m}$ and a depletion depth of about $30\,\mu\mathrm{m}$ are excellent photon detectors in the energy region around 2.9 keV [20,21]. The essential feature is that a photon of 2.9 keV deposits its energy (in 85% of the cases) in one single pixel. Since most background events, which outnumber the true X-ray events by typically four orders of magnitude [9], are multi-pixel (cluster) events, the pionic hydrogen X-ray events can be singled out efficiently by demanding an energy deposit of the appropriate amount in one single pixel.

In a first step of the data analysis, all pixels containing an accumulated charge above a (lower) threshold corresponding to 1.2 keV deposited energy were selected as candidates for an X-ray hit, if the charges of their eight surrounding pixels were consistent with the noise level (single-pixel criterion [22,20]). The $K_{\alpha 1}$ peak of the argon calibration measurement was used for the energy calibration of the measured charge. Figure 3 shows the energy spectra from one of the CCD's, i.e. the number of single pixel events as a function of their accumulated charge, for the pionic hydrogen run, a, the pionic beryllium run, b, and an argon measurement, c. In Figs. 3a,b the electronic K_α lines of aluminium (at 1.5 keV) and silicon (at 1.7 keV) are seen; they originate from the aluminium shielding around the CCD's and the silicon of the CCD's, respectively. Figure 3c shows, in addition to the silicon K_α line, an escape peak at 1.2 keV (an argon K_α X-ray of 2.9 keV produced a hole in the silicon K-shell

[1] In a recent paper [18] ChPT was used to calculate the electromagnetic correction δ_ε. The authors claim that "... $O(p^2)$ calculations in ChPT strongly deviate from the predictions of the potential model" [16]; their result differs from ours by 1.3 standard deviations. Moreover, their result does not contain quantitatively important contributions, such as the mass splitting effect, the γn-channel and the interference between vacuum polarization and strong interaction. In their own words: "It remains to be seen, how the $O(p^2)$ result in ChPT is altered by the loop corrections

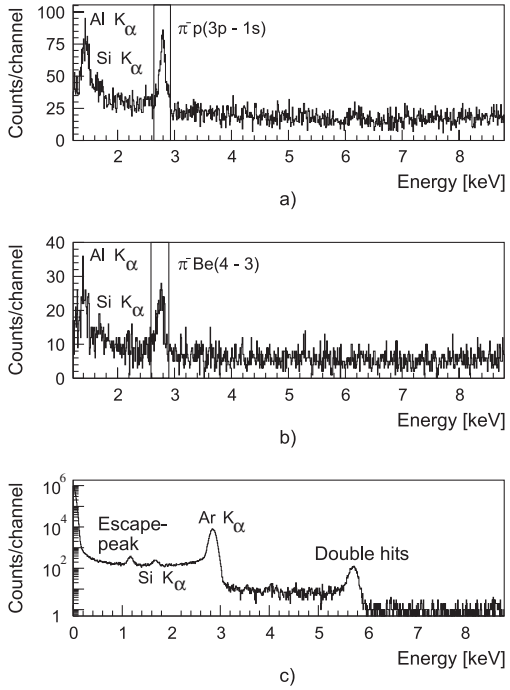

Fig. 3a–c. Energy spectra for one CCD: number of single-pixel events as a function of their accumulated charge, expressed in energy units (1 channel corresponds to 10 eV). **a** Pionic hydrogen; **b** pionic beryllium; **c** argon K_α. (Note that the energy scale in **a** and **b** starts at 1.2 keV)

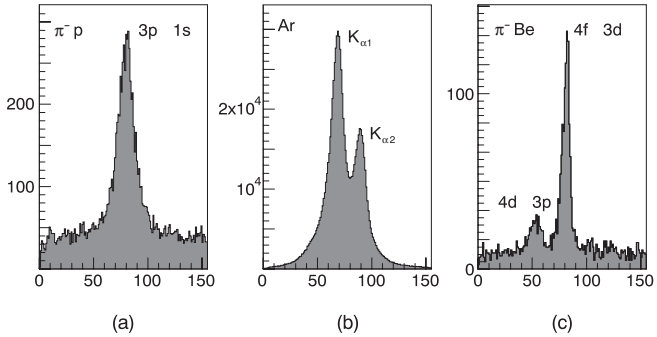

Fig. 4a–c. Position spectra (line profiles): number of single-pixel events with the proper amount of charge, projected on to the x-axis of the CCD's. The units are counts per channel versus channel number. One channel corresponds to 5 pixels. **a** Pionic hydrogen $3p$–$1s$ transition; **b** electronic argon K_α line; **c** pionic beryllium $4f$–$3d$ and $4d$–$3p$ transitions. (One channel is equivalent to 0.088, 0.101 and 0.080 eV for the measurements **a**, **b** and **c**, respectively)

and the subsequently emitted silicon K_α X-ray (1.7 keV) escaped detection) and the "double hit" line produced by two argon K_α X-rays hitting the same pixel.

In the second step of the data analysis, a narrow energy cut around the energy deposited by the pionic X-rays was applied, as shown in Figs. 3a,b. The events within these cuts (vertical lines in the figures) have been used to create the position spectra, i.e. the line profiles for the pionic X-ray analysis. These profiles were obtained by projecting the selected single pixel events onto the local CCD x-axis (Sect. 2.5). The position spectra thus obtained are displayed in Figs. 4, where the line profiles of all (four) CCD's have been added. In this procedure, the position of the CCD's relative to each other and the slight curvature of the profiles were taken into account [9,11]; a binning of five pixels per channel is used. Figure 4a shows the pionic hydrogen $3p$–$1s$ transition, Fig. 4b the electronic argon K_α line and Fig. 4c the pionic beryllium $4f$–$3d$ transition. The broadening of the $3p$–$1s$ X-ray line is clearly visible (comparing Fig. 4a with c).

2.4 The transition line width $\Gamma^{\mathrm{meas.}}_{3p\text{-}1s}$

In order to obtain the instrumental resolution function of the spectrometer from the measured $4f$–$3d$ beryllium line (Fig. 4c), a number of effects of line broadening were investigated and taken into account.

As a first step, the neighboring $4d$–$3p$ line (see Fig. 4c) was removed by fitting to both lines the same analytical function (two Gaussian profiles) and subtracting the weak component.

The $4f$–$3d$ line is broadened by the magnetic dipole and electric quadrupole *hyperfinestructure (hfs) splitting* of the pionic $3d$ state. The hfs splitting of the $4f$ state, however, can be neglected. From the data of [23] the hfs components and the relative intensities of the lines for ^{9}Be have been calculated; the level splittings are between 11 meV and 95 meV [12].

An additional broadening could result from *different electronic K-shell populations* during the various $4f$–$3d$ pionic X-ray decays in the solid state environment (in contrast to a dilute gas where electrons are stripped off the pionic atom). There are three possible states of K-shell occupation, namely zero, one and two K-electrons present. Due to the electron screening of the nuclear charge, the X-ray transition energy is lowered by 96 meV per K-electron present [24]. The electron screening effect would cause a $4f$–$3d$ line broadening if (and only if) more than one K-shell occupation state occurs. An indication of the K-shell populations is obtained by comparing the theoretical $4f$–$3d$ transition energy, calculated for an empty K-shell (2844.193 ± 0.007 eV [25]) with (the center of gravity of) the measured transition energy, namely $2843.974 \pm 0.009(\mathrm{stat.}) \pm 0.043(\mathrm{syst.})$ eV. The difference of 219 ± 50 meV indicates that on the average two K-electrons are present, in which case the shifted lines would be unbroadened. Small contributions from components with zero and one K-shell electron can, however, not be excluded completely.

The $3p$ state is broadened due to its decay width which is dominated by the Auger width of 9 meV (the radiative width is less than 1 meV).

The instrumental resolution function can be described by an analytical function consisting of two Lorentzians with free parameters for height, width and position, i.e. a total of six free parameters. The hfs lines with known separation and relative intensity were fitted (using the resolu-

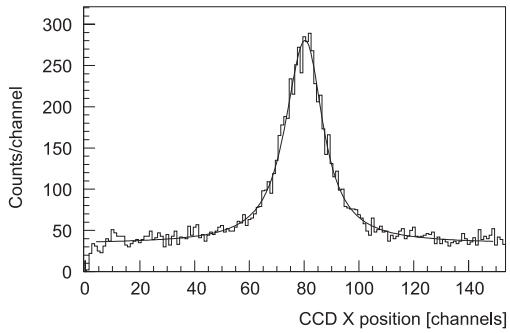

Fig. 5. Best fit to the pionic hydrogen data of the convolution of the natural line shape and the resolution function on a flat background. One channel corresponds to 5 pixels (equivalent to 0.088 eV). (The first and the last 5 channels were not used for the fit because of "blind" pixel lines)

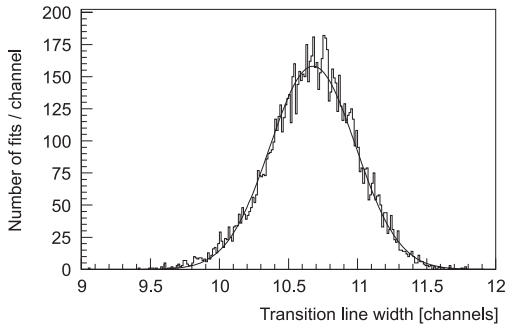

Fig. 6. The pionic hydrogen $3p$–$1s$ transition line width and its uncertainty due to the statistical fluctuations of the resolution function (Monte Carlo study). The number of fits for different resolution functions per unit of energy is shown; one channel corresponds to 0.088 eV

tion function) to the measured $4f$–$3d$ beryllium line. The beryllium line could be described perfectly with a separation of 4.3 channels between the two Lorentzians and an intensity ratio of 1 : 1.6. The FWHM of the complete instrumental resolution function was found to be 7.13 channels, corresponding to 568 meV. (Note that for the deconvolution of the measured pionic X-ray line the whole line shape matters, not merely its width.)

In order to obtain the transition line width $\Gamma^{\text{meas.}}_{3p\text{-}1s}$ and the peak position of the pionic hydrogen $3p$–$1s$ transition, the convolution of a Lorentzian, assumed to describe the line shape of the $3p$–$1s$ transition, with the instrumental resolution function was fitted to the hydrogen data (Fig. 4a), assuming a constant background. Figure 5 shows the best fit to the pionic hydrogen data.

In order to investigate the possible influence of different resolution functions on the transition line width and the peak positions of the various lines, a Monte Carlo study was undertaken. Based on the covariance matrix of the six parameters describing the instrumental resolution function, obtained from the best fit to the beryllium $4f$–$3d$ data, a random sample of 10 000 different parameter sets have been generated, taking the correlations between the parameters explicitly into account. For all sets the convolution of the resolution function with the natural line shape was fitted to the hydrogen and argon data, yielding 10 000 different values for the line width, the peak positions and the corresponding fit errors.

Figure 6 displays the distribution of the widths resulting from the convolution of the 10 000 different resolution functions with the natural hydrogen (single Lorentz) line. A Gaussian fit to this distribution gives the result $\Gamma^{\text{meas.}}_{3p\text{-}1s} = 10.68 \pm 0.31$ channels, corresponding to 0.935 ± 0.027 eV. The quoted error is due to the statistical uncertainty of the resolution function. The fit error was found to be 0.49 channels or 0.043 eV, independent (within 5 meV) of the resolution function. The total statistical error of the width is the quadratic sum of the statistical error of the resolution measurement (Fig. 6) and the fit error (statistical error of the hydrogen measurement). The result is: $\Gamma^{\text{meas.}}_{3p\text{-}1s} = 0.935 \pm 0.051(\text{stat.})$ eV. After correction for the Auger width of the pionic $4f$–$3d$ calibration line

Table 1. Transition line width $\Gamma^{\text{meas.}}_{3p\text{-}1s}$ and *transition energy* $E^{\text{meas.}}_{3p\text{-}1s}$, in units of eV. Statistical and systematic errors are given in the first and second bracket, respectively

$\Gamma^{\text{meas.}}_{3p\text{-}1s}$	$E^{\text{meas.}}_{3p\text{-}1s}$	reference
0.953 (0.051) (0.010)	2885.910 (0.015) (0.031)	this work
1.029 (0.100)	2885.935 (0.028) (0.035)	[9]
0.969 (0.045) (0.010)	2885.916 (0.013) (0.033)	average

$(9 \pm 6$ meV) and taking into account the systematic uncertainty of the electron screening effect $(9 \pm 9$ meV), we obtain the result of this experiment

$$\Gamma^{\text{meas.}}_{3p\text{-}1s} = 0.953 \pm 0.051(\text{stat.}) \pm 0.010(\text{syst.})\,\text{eV}. \quad (5)$$

In Table 1 we compare this value with the result of the earlier experiment [9]; the results are compatible. We obtain the final result by taking the weighted mean:

$$\Gamma^{\text{meas.}}_{3p\text{-}1s} = 0.969 \pm 0.045(\text{stat.}) \pm 0.010(\text{syst.})\,\text{eV}. \quad (6)$$

2.5 The transition energy $E^{\text{meas.}}_{3p\text{-}1s}$

The transition energy is determined from the wave length of the $3p$–$1s$ pionic hydrogen X-ray line which is obtained from a Bragg angle *difference* measurement relative to the electronic argon $K_{\alpha 1}$ X-ray line of known wave length [15].

The bent crystal assembly (Fig. 1) is mounted on a turntable of which the axis of rotation is vertical and lies in the front surface of the central crystal of the lower (bottom) spectrometer (see Fig. 7). The CCD detector system is mounted on an XY cross slide (XY-table) allowing for horizontal motion in the two (perpendicular) directions X and Y. Between successive argon and hydrogen measurements the CCD system is moved on the XY-table from the "argon position" (Fig. 7) to the "hydrogen position". The (space-fixed) target (X-ray source), the turntable and the XY-table are positioned in such a way that the centers of the target, the crystals and the CCD's of the lower spectrometer are all at the same height; they define the

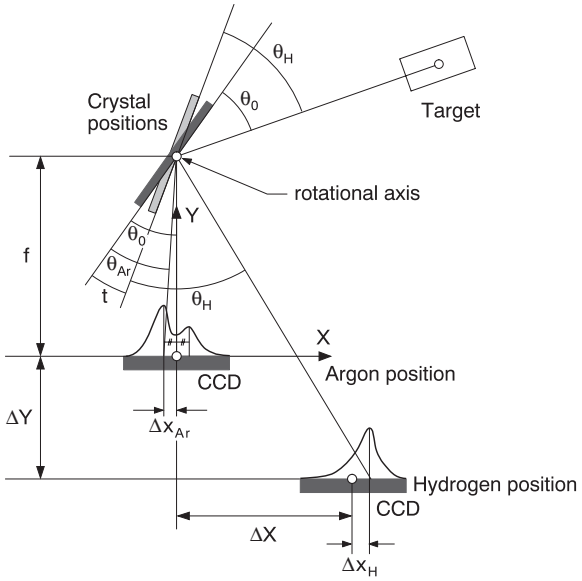

Fig. 7. Geometrical relations between target, bent crystal assembly and CCD detector unit (top view)

horizontal plane $Z = 0$ (called "bottom plane") of a space-fixed spectrometer reference frame (X, Y, Z). The origin O of the reference frame is at the center of the CCD's of the lower spectrometer, at the argon position of the XY-table; the rotational axis of the turntable lies in the YZ plane. In order to have the argon K_α doublet line centered on the CCD, the argon position is defined by the Bragg angle Θ_0 which corresponds to the mean position of the $K_{\alpha 1}$ and $K_{\alpha 2}$ lines (see Fig. 7). The elaborate procedure for properly aligning the crystal assembly on the turntable and the CCD's on the XY-table with respect to the target makes use of a narrow light beam in combination with various optical elements. The individual steps of the alignment procedure are described in [26].

From Fig. 7 we read off the geometrical relations

$$\Theta_{\mathrm{H}} + t = \Theta_0 + \arctan \frac{\Delta X + \Delta x_{\mathrm{H}}}{f + \Delta Y}, \tag{7}$$

$$\Theta_{\mathrm{Ar}} = \Theta_0 + \arctan \frac{\Delta x_{\mathrm{Ar}}}{f}. \tag{8}$$

Here Θ_{H} is the Bragg angle corresponding to the peak position of the $3p$–$1s$ X-ray line of pionic hydrogen, Θ_0 is the Bragg angle corresponding to the mean position between the peaks of the $K_{\alpha 1}$, $K_{\alpha 2}$ X-ray lines of argon, Θ_{Ar} is the Bragg angle of the peak position of the argon $K_{\alpha 1}$ line, t is the angle difference on the turntable between the argon and the hydrogen position, and ΔX and ΔY are the displacements (in X and Y direction) of the XY-table between the two positions. The X-axis of the spectrometer reference frame in the argon position defines the x-axis fixed to the CCD unit with respect to which all position spectra were registered and analyzed. The peak positions Δx_{Ar} and Δx_{H} (Fig. 7) are measured along this x-axis. In the spectra displayed in Figs. 4 and 5, the origin of the x-axis was moved to the left-hand edge of the CCD. The distance f between the rotational axis and the CCD in the argon position (Fig. 7) is directly measured [26] and corresponds to the focal length of the argon K_α X-rays with respect to the bent crystals.

The Bragg angle difference follows from (7) and (8):

$$\begin{aligned}\Delta\Theta_{\mathrm{B}} &\equiv \Theta_{\mathrm{H}} - \Theta_{\mathrm{Ar}} \\ &= \arctan \frac{\Delta X + \Delta x_{\mathrm{H}}}{f + \Delta Y} - \arctan \frac{\Delta x_{\mathrm{Ar}}}{f} - t. \end{aligned} \tag{9}$$

(Note that the angle Θ_0 does not enter.)

Bragg's law in the usual form,

$$\lambda = 2d \sin \Theta_{\mathrm{B}}, \tag{10}$$

does not account for the slight bending of the X-rays in the transition between the material of the crystal and air, nor for the small change of the wave length inside the quartz crystals (refractive index correction). The refractive index correction has been applied as described in [9].

The lattice spacing for the (110) quartz crystals (at 20.5°C) is

$$d = (2.45670 \pm 0.00020)\,\text{Å}. \tag{11}$$

The uncertainty represents the variations of the lattice spacings of the individual crystals. The energy of the argon $K_{\alpha 1}$ line, as measured by Schweppe [15], is

$$E_{K_{\alpha 1}} = (2957.685 \pm 0.019)\,\text{eV}. \tag{12}$$

The data registered with the top spectrometer, with its central plane (called "top plane") inclined by 4° with respect to the bottom plane [9], require a series of additional geometrical corrections (see [26,11]).

From the combined data of both spectrometers, using (11) and (12), the transition energy from this experiment is found to be

$$E^{\mathrm{meas.}}_{3p\text{-}1s} = 2885.910 \pm 0.015(\text{stat.}) \pm 0.031(\text{syst.})\,\text{eV}. \tag{13}$$

Averaging (weighted with the statistical error) with the result from the earlier experiment (see Table 1), we obtain the final result

$$E^{\mathrm{meas.}}_{3p\text{-}1s} = 2885.916 \pm 0.013(\text{stat.}) \pm 0.033(\text{syst.})\,\text{eV}. \tag{14}$$

3 Atomic cascade processes

3.1 Introduction

The pionic atom formation can be described by the simplified capture process in which the orbital motions in the atoms are treated with the Bohr model. In a first phase, the negative pion is slowed down until it reaches the velocity of the atomic electron of hydrogen (with the Bohr radius $r_{\mathrm{B}}(\text{el.})$). The bound electron of hydrogen is then replaced by the negative pion at the distance $r_{\mathrm{B}}(\text{el.})$ from the proton, thus

$$\pi^- + (e^- p)_{n=1} \rightarrow (\pi^- p)_n + e^-. \tag{15}$$

In this process angular momentum and energy are conserved. The principal quantum number of the pionic atom state in (15) is $n \approx (m_\pi/m_e)^{1/2} \approx 15$. Pionic hydrogen in this highly excited state then proceeds through various atomic cascade reactions and decays, until the atom reaches the (initial) $3p$ state from which the observed X-ray is emitted.

Detailed theoretical calculations of cross sections, initial quantum number and kinetic energy distributions for pionic atom formation by negative pions from *molecular* hydrogen have been performed very recently by Cohen [27]. The order of magnitude of the results is nicely reproduced by the simplified process described above.

At the density of the hydrogen target used in the experiment (pressure equivalent to 15 bar), the atomic collisional processes with the neighboring hydrogen molecules dominate by far the radiative transition rates in the upper part of the cascade. Since the average partial lifetime of a pionic atom for radiative decay, e.g. in the state $n = 14$ is about 20 ns (Fig. 7 of [28]; see also [29]), which is comparable to the lifetime of the pion, the much faster atomic processes ensure that the system reaches the $3p$ state before decaying. Despite of their dominance in the upper part of the cascade, the atomic processes have but a small effect on our experimental results. This is related to the fact that (at 15 ρ_{STP}) the pionic hydrogen atom spends most of its lifetime between the collisions in free space. During the short-time collisions with the hydrogen molecules, the pionic atom feels the strong molecular electric fields. One can show with a simple calculation, however, that the shift of the $n = 3$ atomic level due to Stark effect of second order is negligibly small. The broadening of $n = 3$ level due to the first-order Stark effect (no level shift) is also negligible.

In the context of our experiment, there are two main effects of the atomic cascade processes. On the one hand, the Stark effect mixes pionic hydrogen states with different angular momentum l and the same principal quantum number n according to the reaction

$$(\pi^- p)_{nl} + H_2 \rightarrow (\pi^- p)_{nl'} + H_2. \tag{16}$$

This process is called "Stark mixing". From the ns state (the π^- overlaps with the proton), the pionic atom can disappear by the nuclear capture reactions

$$(\pi^- p)_{ns} \rightarrow \pi^0 + n \quad \text{or} \quad \rightarrow \gamma + n. \tag{17}$$

Since at 15 bar the nuclear capture rate is much larger (in the s state) than the Stark mixing rate, the atom always disappears by nuclear capture once the s state is reached. On the other hand, the measured K_β X-ray line shows a small broadening due to the Doppler effect which is the result of several atomic cascade processes (including reaction (15)).

The atomic cascade processes relevant to the present work are listed in Table 2. More details can be found in the recent review by Markushin [29].

Table 2. Processes and corresponding reactions in the pionic atom cascade

Process	Reaction
Nuclear capture	$(\pi^- p)_{ns} \rightarrow \pi^0 + n \quad \text{or} \quad \rightarrow \gamma + n$
Stark mixing	$(\pi^- p)_{nl} + H_2 \rightarrow (\pi^- p)_{nl'} + H_2$
Coulomb deexcitation	$(\pi^- p)_n + H \rightarrow (\pi^- p)_{n'} + H \quad (n' < n)$
External Auger effect	$(\pi^- p)_{n,l} + H_2 \rightarrow (\pi^- p)_{n',l\pm1} + H_2^+ + e^-$
Elastic scattering	$(\pi^- p)_{nl} + H_2 \rightarrow (\pi^- p)_{nl'} + H_2$
Radiative transition	$(\pi^- p)_{n,l} \rightarrow (\pi^- p)_{n',l\pm1} + \gamma$

Table 3. Kinetic energy gain of a pionic hydrogen atom per CD transition, calculated from the binding energy differences $\Delta E^{\pi^- p}_{\mathrm{binding}}$ of the pionic atom states

Transition $n \rightarrow n-1$	$\Delta E^{\pi^- p}_{\mathrm{binding}}$ in eV	Energy gain in eV
$7 \rightarrow 6$	24	11
$6 \rightarrow 5$	39	18
$5 \rightarrow 4$	73	34
$4 \rightarrow 3$	157	73
$3 \rightarrow 2$	450	210

3.2 The Doppler effect

Measurements of the neutron time-of-flight after nuclear capture in liquid hydrogen show a clear Doppler broadening of the $\pi^- p \rightarrow \pi^0 n$ neutrons, corresponding to a kinetic energy distribution of the $\pi^- p$ atom of up to 200 eV at the moment of the pion capture [30,31]. The only cascade process capable of producing such "high energies" is *Coulomb deexcitation* (CD) (see Table 2). This process can be viewed as "inelastic Stark mixing": The pionic-atom state in the molecular electric field mixes with another pionic-atom state of different principal quantum number. (For the reason of energy conservation it must be a state of lower n value.) Assuming that the second hydrogen atom of the molecule acts as a spectator, the released energy is shared almost equally between the pionic atom and the first hydrogen atom. Transitions of the type $n \rightarrow (n-1)$ dominate[2]. Table 3 shows the kinetic energy gained by the pionic hydrogen atom as a result of a CD transition $n \rightarrow (n-1)$.

If a pionic atom at the moment of the $3p$–$1s$ X-ray transition has a kinetic energy of, for instance, 73 eV (following a $4 \rightarrow 3$ CD transition), then the corresponding X-ray energy would be Doppler shifted by a maximum of 1.06 eV. Since this shift is comparable to the decay width of the $1s$ level, it is clear that the investigation of the Doppler effect is important.

As opposed to the CD process, *elastic scattering* between the pionic atom and the surrounding hydrogen molecules (Table 2) leads to a *decrease* in the kinetic energy of the atom.

[2] The Coulomb deexcitation process has been predicted early by Leon and Bethe [32] (see also [33])

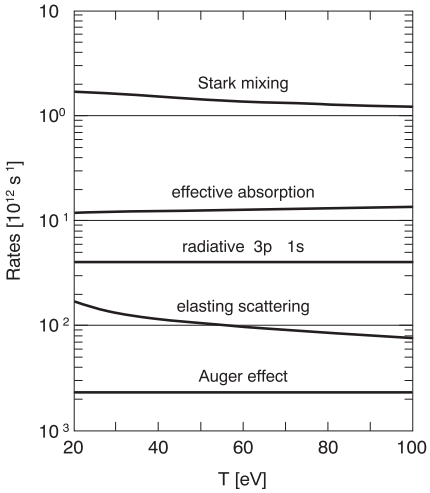

Fig. 8. Rates (transition probability or reaction probability per unit of time) of the main processes in the $n = 3$, $l = 1, 2$ levels of pionic hydrogen, in gaseous hydrogen at 15 ρ_{STP}, as a function of the $\pi^- p$ kinetic energy T. The values are those used in [12], in the atomic cascade code of Markushin et al. [45]

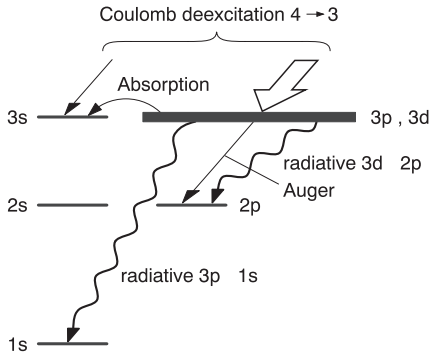

Fig. 9. Schematic diagram for pionic hydrogen showing the population process of the $n = 3$ levels (Coulomb deexcitation $n = 4 \to 3$) and the decay modes of the "mixed" $3p, 3d$ state

It is the interplay between the CD process and elastic scattering which determines the actual Doppler broadening of the $3p$–$1s$ line. The other cascade processes, such as the external Auger process (Table 2), have only small effects on the kinetic energy distribution of the pionic atom.

At present it cannot be excluded that the CD transition could be part of a multi-step process involving molecular hydrogen states [34–36]. Such a possibility is not considered here.

3.3 Recent developments

An improved neutron time-of-flight experiment has recently been performed at PSI [37] in order to obtain (experimentally) more information on kinetic energy distributions of the $\pi^- p$ system in hydrogen targets. In liquid and – most importantly – also in gaseous targets, kinetic energy distributions of the pionic hydrogen atoms have been determined.

On the theoretical side, cross sections for the CD process have recently been calculated by a number of authors [38–43]. The results, however, are partly conflicting. For this reason, we have devised a new method for calculating the Doppler correction which relies as much as possible on *experimental observations* (see Sect. 3.4). Since the density of liquid hydrogen is rather different from that in the (gaseous) hydrogen target of the X-ray experiment, we use for the new method experimental data from *gaseous* hydrogen targets exclusively.

3.4 Calculation of the Doppler correction Δ_{3p}

The Doppler correction Δ_{3p}, defined by (3), is determined here mainly from the neutron time-of-flight experiment [37] with the gaseous hydrogen target (pressure 40 bar) and the X-ray yields measured in a hydrogen target of 15 bar [44]. The theoretical cross sections of the cascade processes (see Fig. 8) are only used weakly, mostly in order to decide about the relative importance of different cascade processes. Whenever absolute values of theoretical cross sections are needed, conservative uncertainty margins are assigned.

(1) Cross sections. Inspection of Fig. 8 shows that the Stark mixing rate dominates by far all other rates. From this fact we conclude that, whenever the $3p$ or the $3d$ state are populated, they are then mixed by the Stark effect *before* any other process occurs. As far as the depopulation of the $3p$ and $3d$ states is concerned, we can therefore assume that both states constitute a complete statistical mixture from which their decay occurs. The mixed $3p$ and $3d$ states are indicated by the rectangle in Fig. 9. Furthermore, Fig. 8 shows that the effective absorption rate dominates over the radiation, elastic scattering, Auger-effect and CD rates. (The CD rate – not shown in Fig. 8 – is below the Auger rate.) The rate for effective absorption is defined as the transition probability per unit of time for a state of the rectangle, to decay by nuclear capture via Stark mixing to the $3s$ state. The decay by absorption is therefore the dominant depopulation mode of the mixed $3p$, $3d$ states, followed by radiative decay and Auger effect (see Fig. 9).

The main cause for the Doppler broadening of the $3p$–$1s$ X-ray transition is the CD process $4 \to 3$, leading to a kinetic energy increase of the atom by 73 eV (Table 3). Let us consider a pionic atom which has just decayed into the $3p$ or $3d$ state by a CD process $4 \to 3$. Since the rate for elastic scattering is much smaller than the effective absorption rate (Fig. 8), the energy loss by elastic scattering with the surrounding hydrogen molecules plays no role; the mixed $3p, 3d$ state will decay with a kinetic energy of 73 eV. The conclusion from this consideration is that, once a pionic atom has gained kinetic energy through the CD process, it will keep it.

(2) CD yields. In this part we aim at a determination of the kinetic energy distribution of the pionic atoms at the moment of the $3p$–$1s$ X-ray transition.

We consider first the population of the statistically mixed $3p, 3d$ states by the CD process $4 \to 3$ (Fig. 9) and calculate the fraction per atom formed (yield) $Y_{K\beta}(73)$ of $3p$–$1s$ X-ray decays whose atoms have acquired an energy of 73 eV. We can write

$$Y_{K\beta}(73) = Y_{\rm CD}(4 \to 3)\frac{8}{9}\frac{\frac{3}{8}\lambda_{K\beta}}{\lambda_{\rm total}(73)}. \qquad (18)$$

Here $Y_{\rm CD}(4 \to 3)$ is the fraction of pionic atoms undergoing a $4 \to 3$ CD transition per pionic atom formed (at the hydrogen target pressure of the experiment). The statistical factor 8/9 (the weight is $(2l+1)$ per l state) is the fraction of pionic atoms (having undergone a $4 \to 3$ CD transition) which decay from a $3p, 3d$ state (Fig. 9). The remaining fraction of 1/9 is transferred (immediately) by Stark mixing to the $1s$ state, before any decay occurs. This follows from the dominance of Stark mixing discussed above. In (18) $\lambda_{K\beta}$ is the rate (transition probability per unit time) for a $3p$–$1s$ X-ray transition and $\lambda_{\rm total}(73)$ is the total decay rate of a mixed $3p, 3d$ state (by absorption, radiation and Auger effect) for a pionic atom with 73 eV kinetic energy. The statistical factor 3/8 is the probability that the $3p$ component of the mixed state is realized. The factor

$$\left(\frac{3}{8}\lambda_{K\beta}\right)/(\lambda_{\rm total}(73))$$

is thus the fraction of $3p$–$1s$ X-rays per decay of the (statistically mixed) $3p, 3d$ state.

The total decay rate can be written as

$$\lambda_{\rm total}(73) = \lambda_{\rm rad}^{\rm total} + \lambda_{\rm abs}(73) + \lambda_{\rm Auger}(73), \qquad (19)$$

where the first term is the total decay rate of the mixed $3p, 3d$ state by radiation, $\lambda_{\rm abs}(73)$ is the effective absorption, i.e. the absorption rate of the mixed $n = 3$ state, and the last term is the Auger decay rate of the (mixed) $3p, 3d$ state. It is understood that all values are to be taken for the hydrogen target density of the present experiment (15 bar). The important term in (19) – apart from the well known radiative rate and the small Auger rate – is the absorption rate. We use the values in Fig. 8 [45,12]

$$\lambda_{\rm abs}(73) = (1.3 \pm 0.7) \times 10^{11}\,{\rm s}^{-1}, \qquad (20)$$

where we have assigned an error band from -50% to $+150\%$, $\lambda_{\rm rad}^{\rm total} = 0.26 \times 10^{11}\,{\rm s}^{-1}$ and $\lambda_{\rm Auger}(73) = 0.02 \times 10^{11}\,{\rm s}^{-1}$. These (quite conservative) errors reflect the uncertainties in the calculations of the effective absorption rate. The values of [45], for which no errors are given, differ by about 25% from the values for $n = 3$ of [32]. It should be noted that both calculations are performed in the "straight-line approximation", assuming no deviation from the straight-line path of pionic hydrogen in its passage through the hydrogen atoms. (In [12] deviations from the straight-line path below kinetic energies of 10 eV are considered; this effect, however, should be small at 73 eV.) The $K\beta$ rate (to be used in (18) [12]) is $\lambda_{K\beta} = 0.398 \times 10^{11}\,{\rm s}^{-1}$.

We intend to use the yield $Y_{\rm CD}(73)$ in (18) from the experiment of [37]. Since that experiment was performed at 40 bar, we have to scale the result to the pressure of the pionic hydrogen experiments (15 bar). This is done by using the cascade code of [45] with parameter values as determined earlier [28,12]. The result is that the yield at 40 bar has to be multiplied by the factor 0.69 in order to obtain the yield at 15 bar.

Table 4. Yields (Y) and fractions (F) of pionic atoms with energies 73, 34 and ≈ 1 eV, respectively, at the instant of the $3p$–$1s$ X-ray transition, and the uncertainties in the Doppler correction from the three groups of energies

E_i [eV]	$Y_{K\beta}(E_i)$	$F_{K\beta}(E_i)$[%]	Uncertainty in Δ_{3p}
73	0.0057	15.1	±0.041
34	0.00088	2.3	±0.008
≈ 1		82.6	±0.017

From the experiment [37], we obtain the yield at 40 bar

$$Y_{\rm CD}(73) = 0.10 \pm 0.04. \qquad (21)$$

The value for this yield quoted in [37] is 0.10 ± 0.02. In order to account for the uncertainty in the pressure scaling factor (0.69), the error was increased to the value given in (21).

All the above values are inserted in (18); they lead to the fraction of $3p$–$1s$ X rays per pionic atom formed[3], having a kinetic energy of 73 eV

$$Y_{K\beta}(73) = 0.0057. \qquad (22)$$

The result (22) is displayed in Table 4.

Next we consider the population of the $3p, 3d$ states (Fig. 9) by the CD process $5 \to 4$, leading to a gain in kinetic energy of 34 eV. As before, we make use of the yield measured by the neutron time-of-flight experiment [37]

$$Y_{\rm CD}(34) = (0.14 \pm 0.06)\%, \qquad (23)$$

where the assigned error again takes account of the uncertainty of the calculated pressure scaling factor. With the same method as before, we calculate the corresponding yield $Y_{K\beta}(34)$ per atom formed. The calculation in this case is somewhat more involved because the effective absorption now takes place from the $n = 4$ as well as the $n = 3$ level. This is also the reason why the yield is considerably smaller than in the former case, in spite of the fact that $Y_{\rm CD}(5\text{–}4)$ and $Y_{\rm CD}(4\text{–}3)$ are comparable in magnitude. We find the value (also shown in Table 4)

$$Y_{K\beta}(34) = 0.00088. \qquad (24)$$

Since the CD processes populating levels with $n > 5$ are expected to be less important for the Doppler broadening of the $K\beta$ X-ray line, we assume that the remaining CD processes contribute to a narrow band of kinetic energy extending from zero to a value of about 1 eV; the energy band is of rectangular shape. These assumptions

[3] The calculation of the uncertainties will be carried out in the next part below

are supported by calculations with the cascade program of [45] (see [12]). In the context of the error calculation of the Doppler correction (see below), the maximum value of the kinetic energy distribution will be varied within certain limits.

Finally, in order to obtain the fraction $F_{K\beta}$ of pionic atoms having a given kinetic energy (see Table 4) from the yields $Y_{K\beta}$, we make use of the (absolute) $K\beta$ X-ray yield (per atom formed) which is reported in [44]:

$$Y_{K\beta}(15\,\mathrm{bar}) = 0.0380 \pm 0.0044. \tag{25}$$

With the value (25) we obtain the fractions $F_{K\beta}(E_i)$ given in Table 4. (The entry in the last line corresponds to a maximum value of the kinetic energy $T_1 = 1\,\mathrm{eV}$.)

(3) Doppler correction. With the kinetic energy distribution of the pionic atoms obtained above we calculate the Doppler broadening of the $K\beta$ X-ray line. The energy distribution consists of three components, a (rectangular) low energy distribution extending from zero to $T_1 = 1\,\mathrm{eV}$ and two discrete peaks at 34 and 73 eV, respectively (Table 4).

The kinetic energy distribution was transformed in the usual way into a Doppler shift distribution for a monochromatic line at the $K\beta$-energy. This distribution was folded with a Lorentzian of width Γ_{1s} corresponding to the total width of the $1s$ state. The value of Γ_{1s} was then varied until the resulting distribution corresponded to the measured line width $\Gamma^{\mathrm{meas.}}_{3p\text{-}1s}$ of the X-ray transition (Table 1). It was shown that the convoluted distribution is again a Lorentzian to a very good approximation. This fact was used in the fitting procedure by which $\Gamma^{\mathrm{meas.}}_{3p\text{-}1s}$ was determined. With this method, the Doppler correction, defined by (3), is found to be

$$\Delta_{3p} = 0.12 \pm 0.05. \tag{26}$$

The error in (26) was determined by varying consecutively the uncertainties of the three components of the kinetic energy distribution, as well as the uncertainty in (25). The maximum value T_1 of the low energy component was varied between 0 eV and 1.8 eV; the latter value is the upper limit of the determination of T_1 from the analysis of the experiment [37] ($T_1 = 1.5 \pm 0.3\,\mathrm{eV}$). The resulting variation in Δ_{3p} is displayed in the last column of Table 4. Also shown in the last column of Table 4 are the variations coming from the uncertainties of $Y_{K\beta}(73)$ and $Y_{K\beta}(34)$, respectively. The variation in Δ_{3p} due to the uncertainty of $Y_{K\beta}(15\,\mathrm{bar})$ is ± 0.014. The quoted error in (26) is the quadratic sum of all variations.

The present value of Δ_{3p} is displayed in Table 5, along with our earlier determinations of the Doppler correction which were based on entirely different methods.

Table 5 shows that the earlier Doppler corrections are not incompatible (within their uncertainties) with the present determination. They are based in part on experiments with liquid hydrogen targets. For the reasons discussed in Sect. 3.3 we adopt the value of the present work.

This section clearly shows that an improved determination of the total decay width Γ_{1s} (3) requires not only an improved experimental determination of the transition line width but also substantial theoretical work on the atomic cascade processes (see also Sect. 4.1).

Table 5. Doppler correction to the measured $3p$–$1s$ transition line width

Δ_{3p}	reference
0.12 ± 0.05	this work
0.07 ± 0.04	[12]
0.05 ± 0.05	[9, 28]

4 Results and conclusions

4.1 Pionic hydrogen

The hadronic πN s-wave scattering amplitudes for elastic scattering and single charge exchange are evaluated from the measured transition energy $E^{\mathrm{meas.}}_{3p\text{-}1s}$ (14) and transition line width $\Gamma^{\mathrm{meas.}}_{3p\text{-}1s}$ (6).

In order to arrive at the strong-interaction shift ε_{1s} (1), we need the electromagnetic transition energy ($E^{\mathrm{el.magn.}}_{3p\text{-}1s}$) [16]; Table 6 shows the various contributions.

With the measured transition energy (14) and the calculated electromagnetic transition energy of Table 6 we obtain the strong-interaction shift (1)

$$\varepsilon_{1s} = -7.108 \pm 0.013(\mathrm{stat.}) \pm 0.034(\mathrm{syst.})\,\mathrm{eV}. \tag{27}$$

Using relation (2), we find with the value (27) the hadronic s-wave scattering amplitude for elastic $\pi^- p$ scattering

$$a_{\pi^- p \to \pi^- p} = (0.0883 \pm 0.0008) m_\pi^{-1}, \tag{28}$$

where statistical and systematic errors were added linearly.

From the measured transition line width $\Gamma^{\mathrm{meas.}}_{3p\text{-}1s}$ (6) and the Doppler correction Δ_{3p} (26) (using relation (3)), we obtain the decay width of the $1s$ state

$$\Gamma_{1s} = 0.868 \pm 0.040(\mathrm{stat.}) \pm 0.038(\mathrm{syst.})\,\mathrm{eV}. \tag{29}$$

With relation (4), using the value (29), we find the hadronic s-wave scattering amplitude for single charge exchange

$$a_{\pi^- p \to \pi^0 n} = (-0.128 \pm 0.006) m_\pi^{-1}. \tag{30}$$

Again, statistical and systematic errors were added linearly.

4.2 Pionic deuterium

From a measurement of the $3p$–$1s$ X-ray transition of pionic deuterium [11] and using the Deser formula [17], we have determined the $\pi^- d$ scattering length [11]. The real part was found to be

$$a_{\pi^- d} = -(0.0259 \pm 0.0011) m_\pi^{-1}. \tag{31}$$

Table 6. Contributions (in eV) to the (calculated) electromagnetic transition energy $E_{3p\text{-}1s}^{\text{el.magn.}}$ [16]

Point-Coulomb, Klein-Gordon equation	2875.715 ± 0.007
Coulomb finite size effect (proton and pion)	-0.102 ± 0.003
Vacuum polarization, order α^2 (Uehling potential, finite size)	3.235 ± 0.001
Higher order contributions (HOC):	
– Relativistic recoil and proton spin and anomalous magnetic moment of the proton	-0.047 ± 0.000
– Vacuum polarization order α^3	0.018 ± 0.000
– Vertex correction	-0.007 ± 0.003
Pionic atom recoil energy	-0.004
$E_{3p\text{-}1s}^{\text{el.magn.}}$	2878.808 ± 0.008

A recent remeasurement of the $1s$ energy shift of pionic deuterium [46] agrees with our value.

In order to combine the results from pionic hydrogen and pionic deuterium one has to establish the relation between $a_{\pi^- d}$ and the πN *isoscalar* and *isovector* (s-wave) *scattering lengths* b_0 and b_1, defined by (33). This relation can be expressed as

$$a_{\pi^- d} = \frac{1 + m_\pi/m_N}{1 + m_\pi/m_d} 2b_0 + a_{\pi^- d}^{(\text{higher order})}, \qquad (32)$$

where in the first term (single scattering in the impulse approximation) $2b_0$ is the sum of the amplitudes for $\pi^- p$ and $\pi^- n$ elastic scattering (see (34)) and $m_{d,N,\pi}$ are the deuteron, nucleon and charged pion masses. The dominating second term in (32) summarizes all remaining (higher order) contributions.

In our previous work [10,9,11], $a_{\pi^- d}^{(\text{higher order})}$ and its dependence on the πN scattering lengths has been taken from the review paper of Thomas and Landau [47] and private communications with Thomas [9].

In the meantime, the problem of relating the $\pi^- d$ scattering length to the πN interaction at threshold has attracted several workers, leading to substantial progress. Baru, Kudryavtsev and Tarasov published results of a systematic investigation based on multiple scattering theory [48,49]. An extensive study of the problem by Ericson, Loiseau and Thomas is in progress [50]; preliminary results have been reported at conferences [51–53]. Moreover, Beane, Bernard, Lee and Meissner have established the relation between the isoscalar πN and the $\pi^- d$ scattering length, to third order in chiral perturbation theory [54].

In view of these recent developments, the calculations of Thomas and Landau [47], which was the basis of our earlier evaluation of the $\pi^- d$ scattering length, is not state of the art anymore, as is discussed in [48].

In our present evaluation of the $\pi^- d$ scattering length, we follow the theoretical work of Baru and Kudryavtsev, supplemented by a recent estimate of these authors for the form factor correction to the double scattering term [55]. We compare our results with the works of Ericson et al. [50] and Beane et al. [54] at the end of Sect. 4.3.

As summarized by Baru and Kudryavtsev [48], there are two main contributions to $a_{\pi^- d}$ from s-wave scattering, namely the first term in (32) (single scattering in the impulse approximation) and the double scattering contribution with the exact πN amplitude and nucleons at fixed centers. In addition, there are two significant terms arising from p-wave $\pi^- N$ scattering, a single scattering contribution and a p- and s-wave interference contribution in double scattering. A small correction for multiple scattering effects was also obtained. The various contributions, all adding up to $a_{\pi^- d}^{(\text{higher order})}$ in (28), are displayed in Table 7. They are calculated with $b_0 = -0.0012 m_\pi^{-1}$, $b_1 = -0.0895 m_\pi^{-1}$ (values close to the scattering lengths), $c_0 = 0.209 m_\pi^{-3}$, $c_1 = 0.177 m_\pi^{-3}$, and taken from Table 3 of [48], representing the average of the "Machleidt 1"- and "Machleidt 2"-deuteron wave functions[4]. The additional correction (not contained in [48]) for non-point-like inter-

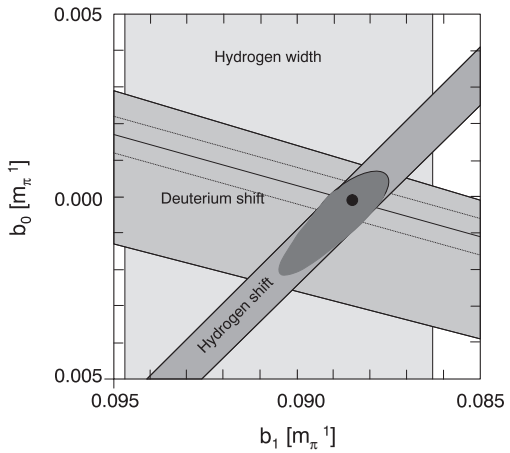

Fig. 10. Constraints on the scattering lengths b_0 and b_1 imposed by the measured strong-interaction shift and width of the $1s$ state of pionic hydrogen and the $1s$ shift of pionic deuterium (details see text)

[4] Note, that the higher order corrections are functions of b_0 and b_1. The values given in Table 7 illustrate the magnitude of the various contributions. These values cannot be used directly to obtain e.g. the central line of the deuterium band in Fig. 10 from (32). The central line of the deuterium band results from constraining the calculated corrections with the value (31), using (32) [48]

Table 7. Contributions to $a_{\pi^- d}^{(\text{higher order})}$ [48] in units of m_π^{-1} (see text)

Double scattering (s-wave)	-0.0254
p-wave single scattering	0.0052
p-s-wave interference in double scattering	-0.0040
multiple scattering	0.0010
(form factor correction	0.0029 [55])
$a_{\pi^- d}^{(\text{higher order})}$	-0.0232

action in double scattering [55], called "form factor correction", is also shown in Table 7 (in parenthesis).

Based on these calculations and the measured value (31) of the $\pi^- d$ scattering length, we have used the relation (32) to establish a constraint between the πN scattering lengths b_0 and b_1. This constraint is shown as the nearly horizontal band in the b_0–b_1 plot of Fig. 10 ("deuterium shift").

The central curve of the band corresponds to $a_{\pi^- d} = -0.0259 m_\pi^{-1}$ (31) and $c = 3m_\pi$ for the off-energy-shell parameter of the deuteron wave function [48]. The upper and the (asymmetrical) lower curve of the deuterium band are estimates of the uncertainty of the theoretical calculations for the higher order terms. For the upper curve we follow [48] and assign the value $c = 3.5m_\pi$ to the parameter of the deuteron wave function. The lower curve corresponds to adding the form factor correction of Table 7 to $a_{\pi^- d}^{\text{higher order}}$, using again the central value $c = 3m_\pi$ for the deuteron wave function parameter. This uncertainty estimate is based on the following argument. According to Kudryavtsev [56], their present value for the form factor correction could be partially canceled by higher order terms. We therefore use (somewhat arbitrarily) their present estimate of the form factor correction to indicate the (present) uncertainty of the theoretical calculations.

The width of the deuterium band in Fig. 10 thus represents the theoretical uncertainties. The uncertainty originating from the deuterium shift measurement (31) is represented by the dotted curves in Fig. 10. The width of the corresponding band is sizeably smaller than the width of the theoretical band and will be neglected.

The slight inclination of the band is mainly due to the dominating double scattering (s-wave) term which is essentially proportional to b_1^2.

The following aspects of the theoretical treatments relating the measured strong-interaction $1s$ energy shift of pionic deuterium to the πN scattering lengths should be kept in mind.

(1) In all theoretical calculations *isospin symmetry of the strong interactions* is assumed.
(2) The $\pi^- d$ scattering length was obtained from the $1s$ energy shift using the Deser formula [17]. This implies that the *electromagnetic corrections* in the pionic deuterium system have been *neglected*. Rockmore [57] has estimated the electromagnetic contributions to the difference of the real parts of the scattering length $a_{\pi^- d}$ and $a_{\pi^+ d}$ to be $-0.0015 m_\pi^{-1}$. This is of the order of the experimental error of $a_{\pi^- d}$, (31).
(3) In the multiple scattering treatment of the relation between $a_{\pi^- d}$ and the πN scattering lengths one problem remains. A complete treatment of the so-called *dispersion* or *absorption correction* is still missing (see discussion at the end of Sect. 4.3).

Despite of the incomplete status of the theory of the $\pi^- d$ system (items (2) and (3)), we will use the present result in the following analysis and discuss the implications in the summary of this paper.

4.3 Isospin symmetry test and the πN scattering lengths

The amplitude of the most general isospin-symmetric πN interaction at threshold is completely determined by two real numbers; it is of the form

$$f_{\pi N} = b_0 + b_1 \boldsymbol{\tau} \cdot \mathbf{t}, \tag{33}$$

where $\frac{1}{2}\boldsymbol{\tau}$ and $\mathbf{t}$ are the nucleon and pion isospin operators, respectively, b_0 is the isoscalar and b_1 the isovector scattering length. These scattering lengths are related to the hadronic s-wave amplitudes for $\pi^- p$ elastic scattering and SCX by

$$a_{\pi^- p \to \pi^- p} = b_0 - b_1 \quad (a_{\pi^- n \to \pi^- n} = b_0 + b_1), \tag{34}$$

and

$$a_{\pi^- p \to \pi^0 n} = \sqrt{2} b_1. \tag{35}$$

In addition to the constraint in the b_0–b_1 plot of Fig. 10 called "deuterium shift" (Sect. 4.2), we obtain two more independent constraints on b_0 and b_1 which are based on the pionic hydrogen measurements. From the elastic scattering amplitude (28), using relation (34), we obtain the second constraint in the b_0–b_1 plot of Fig. 10, designed by "hydrogen shift", and from the SCX amplitude (30), using relation (35), we obtain the constraint called "hydrogen width".

Since all three independent observables were analyzed assuming isospin symmetry of the strong interaction, and because the most general isospin symmetric interaction is determined by *two* (real) scattering lengths, the b_0–b_1 plot of Fig. 10 represents an *isospin symmetry test of the strong interaction* [58]. From the complete compatibility of the three bands of Fig. 10 we conclude that, within present uncertainties, the *strong πN interaction* (at threshold) *is isospin-symmetric*. This statement holds to the level of precision to which b_1 is determined from the hydrogen width, namely 5%.

If we now *assume* isospin symmetry of the strong interaction to hold, then from a common fit to all three constraints in Fig. 10, very precise values for the isoscalar and isovector scattering lengths are obtained. The values are

$$b_0 = (-0.1^{+0.9}_{-2.1}) \times 10^{-3} m_\pi^{-1}, \tag{36}$$

$$b_1 = (-88.5^{+1.0}_{-2.1}) \times 10^{-3} m_\pi^{-1}. \tag{37}$$

Table 8. Chiral perturbation theory contributions to the scattering lengths b_0 and b_1 (from [3]), in units $10^{-3}m_\pi^{-1}$

	1st order	2nd order	3rd order	experiment
b_0	0	LEC's dependent	8.6	$-0.1^{+0.9}_{-2.1}$
b_1	−79.0	0	LEC's dependent	$-88.5^{+1.0}_{-2.1}$

Since the uncertainties in (36) and (37) are at the 1% level (of b_1), the assumption stated above is relevant; the scattering lengths (36), (37) thus represent "isospin-symmetric" values. The scattering lengths (36), (37) are correlated (see Fig. 10).

For completeness we also give the scattering lengths deduced from the two hydrogen observables alone (i.e. without inclusion of the deuterium data): $b_0 = -(2.2 \pm 4.3) \times 10^{-3}m_\pi^{-1}$; $b_1 = -(90.5 \pm 4.2) \times 10^{-3}m_\pi^{-1}$. Note the strong correlation between b_0, b_1 in this case; the correlation coefficient is $\rho_{01} = 0.98$.

It is interesting to confront our values (36) and (37) with evaluations of the scattering lengths with heavy baryon chiral perturbation theory [3]. At threshold, the chiral perturbation series is an expansion in powers of the strong-interaction pion mass M_π. The first-order contribution is the current-algebra prediction of Weinberg:

$$b_0 = 0, \quad b_1 = -\frac{1}{8\pi F_\pi^2}\frac{1}{1+m_\pi/m_N}M_\pi, \qquad (38)$$

where $F_\pi = 92.42 \pm 0.26\,\mathrm{MeV}$ [59] is the pion decay constant, M_π is taken to be the charged pion mass (m_π) and m_N ($= m_{\mathrm{Proton}}$) is the nucleon mass. Some of the higher order terms depend on low-energy constants (LEC's) for which there is no theoretical prediction, whereas others are calculable.

Table 8 shows the individual contributions (up to 3rd order[5]) to the scattering lengths b_0 and b_1, together with our experimental values (32) and (33).

The following observations can be made.

(1) The current-algebra limit (1st order) is close to the actual values of both scattering lengths.
(2) The difference between the 3rd order term and b_0 is larger than the magnitude of b_0 itself, indicating a convergence problem in the heavy-baryon chiral perturbation series – even at threshold.
(3) The scattering lengths b_0, b_1 should provide stringent constraints to the LEC's entering the problem.

Finally, we address other recent determinations of the scattering lengths.

First we compare the (unpublished) work of Ericson, Loiseau and Thomas with our results. Their determination uses as experimental inputs the two shift measurements only. The (unpublished) values for the scattering lengths are [50]: $b_0 = (-1.2 \pm 0.8) \times 10^{-3}m_\pi^{-1}$ and $b_1 = (-89.5 \pm 1.3) \times 10^{-3}m_\pi^{-1}$ (the two errors given in [50] are added quadratically). These values are compatible with ours, although there are differences in the calculations relating the scattering lengths of the $\pi^- d$ to the πN system [50]. The main difference seems to be that the p–s-wave interference term (-0.0040 in Table 7) is small in their work and a dispersion correction (absorption effect) of -0.0056 (in the same units) is added to $a_{\pi^- d}^{(\mathrm{higher\,order})}$. The fact that the calculated values of these effects in the two theoretical procedures are very similar may not be entirely accidental. The p–s-wave interference term could contain at least part of the absorption effect [55].

Table 9. Values for the dispersion integral J (40)

J[mb]	reference
−1.072	[61]
−1.05	[62]
−1.051	[63]
$-1.058^{+0.008}_{-0.014}$	average

We now turn to the work of Beane et al. [54]. As mentioned earlier, these authors have established – in third order chiral perturbation theory – the relation between the scattering lengths $a_{\pi^- d}$ and b_0. From their (7) one has $a_{\pi^- d}^{(\mathrm{higher\,order})} = -0.0203m_\pi^{-1}$. Using (32) and (31) we obtain $b_0 = -(2.6 \pm 0.5) \times 10^{-3}m_\pi^{-1}$ (their (8)). This result again is compatible with ours. One should keep in mind, however, that this value is of limited precision, because the (dominant) double scattering term is treated to lowest order only.

4.4 πN coupling constant and Goldberger–Treiman discrepancy

The isovector scattering length b_1 is related to the πN coupling constant f by the GMO sum rule [60]

$$f^2 = \frac{1}{2}\left(1 - \left(\frac{m_\pi}{2m_N}\right)^2\right)\left[\left(1+\frac{m_\pi}{m_N}\right)m_\pi(-b_1) - m_\pi^2 J\right], \qquad (39)$$

where J is an integral over the difference between $\pi^\pm p$ total cross sections

$$J = \frac{1}{4\pi^2}\int_0^\infty \frac{\sigma_{\pi^- p} - \sigma_{\pi^+ p}}{\sqrt{q^2+m_\pi^2}}\mathrm{d}q. \qquad (40)$$

(q is the laboratory momentum.) With the value of the integral (40) – using the relation (39) – the πN coupling constant f^2 can be determined from the scattering length b_1. Numerically, the relation (39) reads (with $m_N = m_{\mathrm{Proton}}$)

$$f^2 = 0.5712m_\pi(-b_1) - 0.02488\,(\mathrm{mb}^{-1}J). \qquad (41)$$

Table 9 shows recently published results of evaluations of the integral (40).

The uncertainty assigned to the average of the dispersion integral is such that all quoted values are inside the error band[6].

[5] Recently calculations up to 4th order have been performed [6]

[6] The (unpublished) value of Ericson et al. [50] for the dispersion integral is $J = -1.083 \pm 0.009 \pm 0.031\,\mathrm{mb}$

With the value (37) of the isovector scattering length and the average from Table 9, we obtain from relation (41) the πN coupling constant

$$f^2 = 0.0769^{+0.0012}_{-0.0006}. \tag{42}$$

It is interesting to compare this value with two other recent determinations of the πN coupling constant. The most recent partial-wave and dispersion relation analysis value of the VPI/GW group (preliminary analysis) is [64] $f^2 = 0.0760 \pm 0.0001(\text{stat.}) \pm 0.0004(\text{syst.})$. The analysis of the low-energy πN scattering data based on the extended tree-level model of the πN interaction yields the value [65] $f^2 = 0.0766 \pm 0.0011$. The results of all three determinations agree perfectly.

The Goldberger–Treiman (GT) relation is an important tool for testing chiral symmetry of QCD [66]. The GT relation connects the πN coupling constant with the axial charge of the nucleon; it may be written as

$$g_{\pi N} = \frac{g_A m_N}{F_\pi}(1 + \Delta_{\rm GT}), \tag{43}$$

where

$$g_{\pi N} = \frac{2m_N}{m_\pi}\sqrt{4\pi} f = 13.21^{+0.11}_{-0.05} \tag{44}$$

(in (44) the value (42) for f is used), and

$$g_A = 1.2670 \pm 0.0035 \tag{45}$$

is the nucleon axial vector coupling constant [67]. The GT discrepancy $\Delta_{\rm GT}$ is zero in the limit of vanishing quark masses. Using the values (44), (45) and (46) we obtain from (43) the GT discrepancy

$$\Delta_{\rm GT} = 0.027^{+0.012}_{-0.008}. \tag{46}$$

This result may be compared with Leutwyler's estimate [66]: $\Delta_{\rm GT} \simeq 0.02$. We should emphasize that this comparison implies isospin symmetry of the strong interaction.

4.5 The nucleon sigma term

The determination of the sigma term is still a controversial issue [68]. In this section we discuss the *change* of the sigma term as a result of the new values of the scattering length b_0 and the πN coupling constant, with respect to the Karlsruhe–Helsinki (KH) partial wave solution [69]. (All early determinations of the sigma term are based on the KH solution [70–72].)

The nucleon sigma term is defined as the scalar form factor ($\sigma(0)$) of the nucleon at zero momentum transfer [68] and is of particular importance because it represents the response of the nucleon mass to a change in the quark masses [66]. The nucleon sigma term is experimentally accessible through πN scattering. The connection is provided by the isospin even D amplitude (from which the pseudovector Born term is subtracted) $\overline{D}^+$, taken at the unphysical Cheng–Dashen point:

$$\Sigma \equiv F_\pi^2 \overline{D}^+(\nu = 0, t = 2m_\pi^2). \tag{47}$$

According to a low energy theorem, Σ is nearly equal to the scalar form factor of the nucleon at $t = 2m_\pi^2$ [68]:

$$\Sigma = \sigma(2m_\pi^2) + \Delta_{\rm R}, \quad 0 < \Delta_{\rm R} < 2\,\text{MeV}. \tag{48}$$

One then obtains $\sigma(0)$ from Σ, see (48), and the relation $\sigma(2m_\pi^2) - \sigma(0) \simeq 15\,\text{MeV}$ (which is assumed to be well known [66]).

The dominant piece of Σ is given by the first two terms in the subthreshold expansion of the $\overline{D}^+$ amplitude

$$\overline{D}^+(\nu = 0, t) = d_{00}^+ + d_{01}^+ \cdot t + \cdots \tag{49}$$

We write (47) as

$$\Sigma = \Sigma_d + \Delta_D, \tag{50}$$

where

$$\Sigma_d = F_\pi^2(d_{00}^+ + 2m_\pi^2 d_{01}^+), \tag{51}$$

and $\Delta_D \simeq 12\,\text{MeV}$ [71] is due to the higher order terms in (49) and is assumed to be well known. The determination of the sigma term is thus reduced to a determination of the subthreshold parameters d_{00}^+ and d_{01}^+.

These coefficients have been expressed from dispersion relations as [71,68]

$$d_{00}^+ = \overline{D}^+(m_\pi, 0) + J_D(0), \quad d_{01}^+ = \overline{E}^+(m_\pi, 0) + J_E(0), \tag{52}$$

where $J_D(0)$, $J_E(0)$ are dispersion integrals. The subtraction constants $\overline{D}^+(m_\pi, 0)$, $\overline{E}^+(m_\pi, 0)$ depend on the scattering length $a_{0+}^+ \equiv b_0$, the scattering volume a_{1+}^+ and the πN coupling constant:

$$\overline{D}^+(m_\pi, 0) = 4\pi(1 + x)b_0 + \frac{g_{\pi N}^2 x^3}{m_\pi(4 - x^2)}, \tag{53}$$

$$\overline{E}^+(m_\pi, 0) = 6\pi(1 + x)a_{1+}^+ - \frac{g_{\pi N}^2 x^2}{m_\pi^3(2 - x)^2}, \tag{54}$$

where $x = m_\pi/m_N$.

If we insert the KH values from Table 2.4.7.2 of [69], $b_0 = -0.010 m_\pi^{-1}$, $a_{1+}^+ = 0.133 m_\pi^{-3}$, using the relations (52), (53), (54) as given in [71] in numerical form, we obtain

$$\Sigma_d = 48\,\text{MeV}. \tag{55}$$

We now determine the differences to Σ_d which arise from the new values of b_0 (36) and f^2 (42), relative to the KH values $b_0 = -0.010 m_\pi^{-1}$ and $f^2 = 0.079$. These differences $\Delta\Sigma_d$ will be independent of the values of the dispersion integrals in (52) and of a_{1+}^+ in (54). From (51), (52), (53), (54) we find with (36) and (42)

$$\Delta\Sigma_d(b_0) = \left(9^{+1}_{-2}\right)\,\text{MeV}, \quad \Delta\Sigma_d(g_{\pi N}) = \left(4^{+1}_{-2}\right)\,\text{MeV}. \tag{56}$$

The errors assigned to the values in (56) reflect our uncertainties on b_0 and f^2.

From this analysis we conclude that the nucleon sigma term is sizeably *increased* as a result of the new values of b_0 and f^2, by

$$\Delta\Sigma_d = \Delta\Sigma_d(b_0) + \Delta\Sigma_d(g_{\pi N}) = \left(13^{+2}_{-4}\right)\,\text{MeV}, \tag{57}$$

relative to the determinations based on the KH solution[7]. Such an increase is not easy to account for theoretically [68].

4.6 Summary and outlook

In the pionic hydrogen part of this paper, we describe our last X-ray experiment, summarize the present knowledge on the atomic cascade processes leading to the Doppler correction factor and deduce the (πN) s-wave $\pi^- p$ elastic and SCX scattering amplitudes at threshold. In the part on pionic deuterium we summarize the present knowledge on the theoretical relation between the $\pi^- d$ scattering length and the πN scattering amplitude, use our earlier experimental result on the $\pi^- d$ scattering length and deduce a constraint on the isoscalar (b_0) and isovector (b_1) πN (s-wave) scattering lengths. We then combine the information from pionic hydrogen and deuterium and obtain the following results:

(1) The measured scattering lengths are consistent with the isospin symmetry of the strong πN interaction at threshold, at the level of 5% (relative to b_1).
(2) Under the assumption of isospin symmetry, the s-wave scattering lengths b_0 and b_1 are determined at the 1–2% level.
(3) The scattering lengths are remarkably close to the current-algebra prediction.
(4) The b_0 value indicates a convergence problem in the heavy-baryon chiral perturbation series.
(5) From b_1 the πN coupling constant

$$f^2 = 0.0769^{+0.0012}_{-0.0006}$$

is obtained.
(6) The corresponding Goldberger–Treiman discrepancy is

$$\Delta_{\mathrm{GT}} = \left(2.7^{+1.2}_{-0.8}\right)\,\%.$$

(7) The sigma term Σ_d is larger by at least 9 MeV as compared to the KH value.

At the level of the scattering amplitudes, precisions reached from our experiments are at the 1% level, which seems to be unique in hadron physics. Unfortunately, these precisions cannot be fully exploited because there seems to be a lack of consensus among the theorists working on the $\pi^- d$ system, e.g. on the issues of absorption and form factor corrections. It should also be stressed that no systematic treatment of the electromagnetic corrections on the $\pi^- d$ system is yet available. In view of the important results shown here, it should be tempting to do more theoretical work on the $\pi^- d$ system in order to improve our present knowledge on such important items as the πN coupling constant and the sigma term.

On the experimental side, a new collaboration has been formed at PSI to continue precision X-ray experiments on pionic hydrogen and deuterium. In their recent proposal [74], the ambitious goal of measuring both, shift *and* width of pionic hydrogen at the 1% level is formulated.

[7] See also the discussion on the sigma term in [73]

Acknowledgements. We would like to thank Leo Knecht, Bruno Leoni and Hermann Obermeier for their contributions to the design and construction of the spectrometer system, and Daniel Varidel and Patrick Pollet for designing and building the CCD and associated electronics. Clarifying and interesting discussions with Vadim Baru, Thomas Becher, Torleif Ericson, Jürg Gasser, Joachim Kambor, Alexander Kudryavtsev, Heinrich Leutwyler, Nadia Fettes, Anatoli Gridnev, Valeri Markushin, Ulf Meissner and Akaki Rusetsky are acknowledged. The high quality beam at PSI, delivered by the competent accelerator and technical staff, was essential for the success of our experiments. The research was supported in part by the Swiss National Science Foundation.

References

1. H. Leutwyler, in Chiral dynamics: theory and experiment, edited by A.M. Bernstein, B.R. Holstein (Springer 1995), p. 14
2. J. Gasser, M.E. Sainio, A. Svarc, Nucl. Phys. B **307**, 779 (1988)
3. M. Mojzis, Eur. Phys. J. C **2**, 181 (1998)
4. N. Fettes, U.-G. Meissner, S. Steininger, Nucl. Phys A **640**, 199 (1998)
5. T. Becher, H. Leutwyler, Eur. Phys. J. C **9**, 643 (1999)
6. N. Fettes, U.-G. Meissner, Nucl. Phys. A **676**, 311 (2000)
7. N. Fettes, U.-G. Meissner, Phys. Rev. C **63**, 045201 (2001)
8. N. Fettes, U.-G. Meissner, Nucl. Phys. A **679**, 629 (2001)
9. D. Sigg et al., Phys. Rev. Lett. **75**, 3245 (1995); D. Sigg et al., Nucl. Phys. A **609**, 269 (l996); Erratum A **617**, 526 (1997)
10. H.-Ch. Schröder et al., Phys. Lett. B **469**, 25 (1999)
11. D. Chatellard et al., Phys. Rev. Lett. **74**, 4157 (1995); D. Chatellard et al., Nucl. Phys. A **625**, 855 (l997)
12. H.-Ch. Schröder, Ph.D. thesis ETH Zurich, No. 11760, 1996
13. A. Badertscher et al., Nucl. Instr. and Meth. A **335**, 470 (1993)
14. L.M. Simons, Phys. Scr. T **22**, 90 (1988)
15. J. Schweppe, National Institute for Standards and Technology (NIST), Gaithersburg, Washington DC, USA, private communication, 1994
16. D. Sigg, A. Badertscher, P.F.A. Goudsmit, H.J. Leisi, G.C. Oades, Nucl. Phys. A **609**, 310 (1996)
17. S. Deser et al., Phys. Rev. **96**, 774 (1954)
18. V.E. Lyubovitskij, A. Rusetsky, Phys. Lett. B **494**, 9 (2000)
19. J. Spuller et al., Phys. Lett. B **67**, 479 (1977)
20. D. Varidel et al., Nucl. Instr. and Meth. A **292**, 147 (1990)
21. G. Fiorucci et al., Nucl. Instr. and Meth. A **292**, 141 (1990)
22. D. Sigg, Nucl. Instr. and Meth. A **345**, 107 (1994)
23. R. Beetz et al., Nucl. Phys. A **300**, 369 (1978); Tables of Isotopes, edited by C.M. Lederer, V.S. Sherley (John Wiley and Sons 1978)
24. B. Aas et al., Nucl. Phys. A **373**, 405 (1982)
25. B. Jeckelmann, IMP-ETHZ Internal Report LB-85-03, 1985
26. D. Sigg, Ph.D. thesis ETH Zurich, No. 11049, 1995
27. J.S. Cohen, Phys. Rev A **59**, 4300 (1999)
28. E.C. Aschenauer et al., Phys. Rev. A **51**, 1965 (1995)
29. V.E. Markushin, Hyperfine Interactions **119**, 11 (1999)

30. J.F. Crawford et al., Phys. Rev. Lett. **56**, 1043 (1986); Phys. Lett. B **213**, 391 (1988); Phys. Rev. D **43**, 46 (1991)
31. A. Badertscher et al., Phys. Lett. B **392**, 278 (1997)
32. M. Leon, H.A. Bethe, Phys. Rev. **127**, 636 (1962)
33. L. Bracchi, G. Fiorentini, Nuovo Cimento A **43**, 9 (1978)
34. D. Taqqu, in AIP Conference Proceedings 181, edited by S.E. Jones et al. (Amer. Inst. Phys., New York 1989) p. 217
35. P. Froelich, J. Wallenius, Phys. Rev. Lett. **75**, 2108 (1995)
36. S. Jonsell, J. Wallenius, P. Froelich, Phys. Rev. A **59**, 3440 (1999)
37. A. Badertscher et al., Europhys. Lett. **54**, 313 (2001)
38. L.I. Menshikov, L.I. Ponomarev, Z. Phys. D **2**, 1 (1985)
39. W. Czaplinsky et al., Muon Catalyzed Fusion **2**, 59 (1990/91)
40. W. Czaplinsky et al., Phys. Rev. A **50**, 525 (1994)
41. L.I. Ponomarev, E.A. Solov'ev, JETP Lett. **64**, 135 (1996)
42. L.I. Ponomarev, E.A. Solov'ev, Hyperfine Interaction **119**, 55 (1999)
43. A. Kravtsov, Hyperfine Interaction **119**, 45 (1999)
44. A.J. Rusi El Hassani et al., Z. Phys. A **351**, 113 (1995)
45. V.E. Markushin et al., Muon Catalyzed Fusion **7**, 155 (1992)
46. P. Hauser et al., Phys. Rev. C **58**, R1869 (1998)
47. A.W. Thomas, R.H. Landau, Physics Report **58**, 121 (1980)
48. V.V. Baru, A.E. Kudryavtsev, Physics of Atomic Nuclei **60**, 1475 (1997)
49. V.E. Tarasov, V.V. Baru, A.E. Kudryavtsev, Physics of Atomic Nuclei **63**, 801 (2000)
50. T.E.O. Ericson, B. Loiseau, A.W. Thomas, hep-ph/0009312
51. B. Loiseau, T.E.O. Ericson, A.W. Thomas, πN Newsletter No. 15, December 1999, p. 162
52. T.E.O. Ericson, B. Loiseau, A.W. Thomas, Nucl. Phys. A **663, 664**, 541c (2000)
53. T.E.O. Ericson, B. Loiseau, A.W. Thomas, Physica Scripta T**87**, 71 (2000)
54. S.R. Beane et al., Phys. Rev. C **57**, 424 (1998)
55. A.E. Kudryavtsev, private communication, March 2000
56. A.E. Kudryavtsev, private communication, June 2000
57. R.M. Rockmore, Phys. Lett. B **356**, 153 (1995)
58. H.J. Leisi et al., in Chiral dynamics: theory and experiment, edited by A.M. Bernstein, B.R. Holstein (Springer, 1995) p. 241
59. Particle Data Group, Eur. Phys. J. C **15**, 395 (2000)
60. M.L. Goldberger, H. Miyazawa, R. Oehme, Phys. Rev. **99**, 986 (1955)
61. R.L. Workman et al., Phys. Rev. Lett. **68**, 2712 (1992) (erratum)
62. R.A. Arndt et al., Phys. Rev. C **52**, 2120 (1995)
63. W.R. Gibbs, W.B. Kaufmann, Phys. Rev. C **57**, 784 (1998)
64. M.M. Pavan et al., πN Newsletter No. 15, December 1999, p. 171
65. E. Matsinos, Phys. Rev. C **56**, 3014 (1997)
66. H. Leutwyler, πN Newsletter No. 15, December 1999, p. 1
67. Particle Data Group, Eur. Phys. J. C **15**, 695 (2000)
68. M. Knecht, πN Newsletter No. 15, December 1999, p. 108
69. G. Höhler, Pion-nucleon scattering, Landolt-Börnstein, Vol. I/9b2, edited by H. Schopper (Springer, Berlin 1983)
70. R. Koch, Z. Phys. C **15**, 161 (1982)
71. J. Gasser et al., Phys. Lett. B **213**, 85 (1988)
72. J. Gasser et al., Phys. Lett. B **253**, 252 (1991)
73. H.J. Leisi, in PSI Proceedings 98-02, December 1998, edited by D. Graudenz, ISSN 1019-6447 p. 33
74. D. Gotta, πN Newsletter No. 15, December 1999, p. 276